Journal of Alloys and Compounds 513 (2012) 236–241

Contents lists available at SciVerse ScienceDirect

Journal of Alloys and Compounds

journal homepage: www.elsevier.com/locate/jallcom

Rate performance of $Li_3V_2(PO_4)_3$/C cathode material and its Li^+ ion intercalation behavior

Feng Wu, Feng Wang, Chuan Wu*, Ying Bai

Beijing Key Laboratory of Environmental Science and Engineering School of Chemical Engineering and the Environment, Beijing Institute of Technology, Beijing 100081, China

ARTICLE INFO

Article history:
Received 9 July 2011
Received in revised form 9 October 2011
Accepted 11 October 2011
Available online 18 October 2011

Keywords:
Lithium vanadium phosphate
High power
Diffusion coefficient
Cathode

ABSTRACT

Rate performance and kinetic properties of $Li_3V_2(PO_4)_3$/C composite electrode have been investigated in this paper. The $Li_3V_2(PO_4)_3$/C composite obtained via a rheological phase method displays a monoclinic structure with an average particle size of ca. 200–300 nm. Electrochemical tests show this material exhibits good reversibility and excellent rate capability up to a current density of 3373 mA g^{-1} (30 C). The composite material achieves its theoretical capacity at 1 C rate. The capacity loss is less than 4% from 1 to 10 C. Even at the highest 30 C rate, the capacity is above 100 mAh g^{-1}. The kinetic properties of the composite electrode are analyzed by cyclic voltammetry (CV) and potentiostatic intermittent titration (PITT) techniques. The Li^+ ion diffusion coefficients calculated from PITT are in the range of 10^{-7}–10^{-8} cm^2 s^{-1}.

1. Introduction

Rechargeable lithium batteries have become of great importance in our life which has never been so dependant on portable digital devices. Nevertheless, the development of battery systems is far behind the ever-updating terminals. As the pace of electric vehicles accelerates, researchers are eager to find electrode materials with both thermal stability and high power density. Recently, monoclinic $Li_3V_2(PO_4)_3$ is emerging as a promising high-power material which boasts both high voltage plateaus and fast ion mobility [1–5]. As a member of polyanion compounds, $Li_3V_2(PO_4)_3$ also possesses outstanding electrochemical and thermal stability [6], which makes it rather appleaing.

Extraction of all Li from $Li_3V_2(PO_4)_3$ corresponds to a maximum capacity of 197 mAh g^{-1} and an average potential of ~4 V (vs. Li/Li^+). Numerous efforts have been made to enhance the performance of $Li_3V_2(PO_4)_3$ [7–16]. The electrochemical behavior could be improved by selecting proper synthesis routes and/or carbon sources, attempting to ameliorate mixing effect and/or control particle morphology. Wang et al. [9] reported that $Li_3V_2(PO_4)_3$/C prepared via a PVA-assisted ball-milling route delivered long-term cyclability. Qiao et al. [13] prepared plate-like $Li_3V_2(PO_4)_3$/C via a glycine-assisted solution route, which showed a high reversible capacity. The above results were based on the utilization of two Li, associated with the V^{3+}/V^{4+} redox couple. The reversible cycling of three Li from $Li_3V_2(PO_4)_3$, though theoretically possible according to phase identification [17,18], is problematic. Previous literature [10–14] showed that $Li_3V_2(PO_4)_3$ exhibited a quick capacity fade in early cycles when charged up to 4.8 V, and this problem seemed irrelavant with synthesis routes or raw materials. The underlying mechanism is not clear yet. We focus on the cycling of two Li from $Li_3V_2(PO_4)_3$ in the present study aiming to achieve better rate performance.

The Li^+ ion diffusion coefficient is one of the most important parameters revealing the kinetic properties of Li-insertion hosts. Li^+ transport is mainly dependant on the crystallographic structure of insertion hosts. However, particle morphology also matters since it could affect the diffusion length and mutual contact. Linear potential sweep voltammetry can provide only values of D_{Li} around the voltammetric peaks [19]. To further observe the changes of diffusion coefficients in the intercalation process, we chose the PITT method. PITT can provide more detailed results, which enables us to get a panoramic view of the diffusion coefficients. The classical application of PITT is usually related to systems in which the concentration of intercalants changes monotonically as intercalation proceeds. Such systems (e.g., graphite materials) undergo solid-state intercalation reactions which lead to the formation of solid-solution phases during the intercalation process [19]. However, this technique has also been applied to intercalation systems with two-phase reactions [19–21]. In such situations, the diffusion coefficient mainly reflects attractive interactions between the intercalation species [22]. In this paper, CV and PITT were used to analyze the Li^+ ion diffusion behavior of $Li_3V_2(PO_4)_3$/C composite electrode.

* Corresponding author. Tel.: +86 10 68912657.
E-mail address: chuanwu@bit.edu.cn (C. Wu).

0925-8388/$ – see front matter © 2011 Elsevier B.V. All rights reserved.
doi:10.1016/j.jallcom.2011.10.028

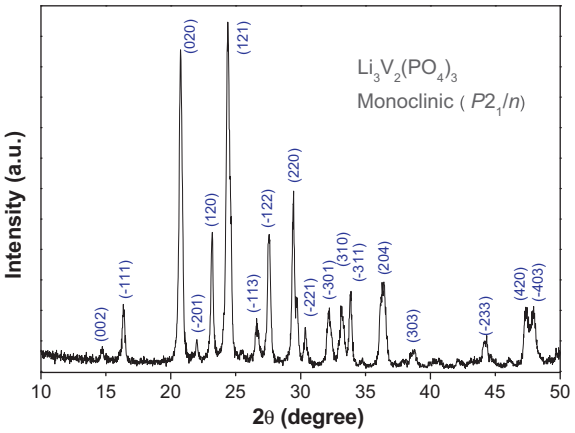

Fig. 1. X-ray diffractogram of the $Li_3V_2(PO_4)_3$/C composite prepared via rheological phase method.

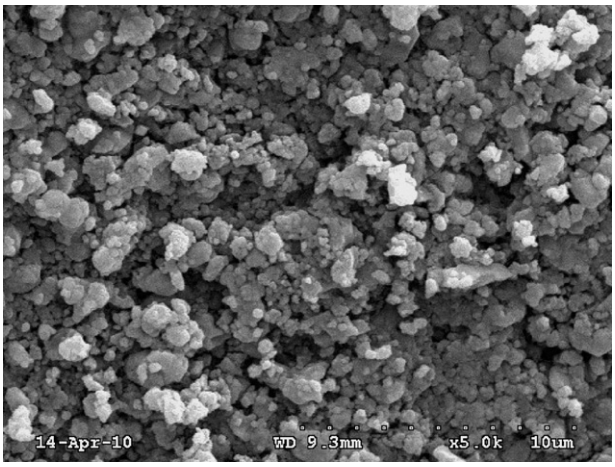

Fig. 2. SEM image of $Li_3V_2(PO_4)_3$/C particles.

2. Experimental

The $Li_3V_2(PO_4)_3$/C composite was prepared via a rheological phase method [23–25]. All chemicals used were of analytical grade. Stoichiometric amounts of $LiOH{\cdot}H_2O$, NH_4VO_3, and $NH_4H_2PO_4$ were added to a Teflon container. Citric acid equivalent mole to NH_4VO_3 was employed as both chelating reagent and carbon source. Then a small amount of deionized water was added dropwise into the container to form a rheological mixture, followed by magnetic stirring for 15 min. The container was then sealed in a stainless autoclave and placed in an oven at 80 °C for 8 h. The obtained precursor was dried, ground, and heated at 350 °C with flowing argon for 4 h. The resulting powders were then reground, pressed into pellets, and annealed at 850 °C for 4 h under argon flow.

The crystallographic structure of the product was characterized by X-ray diffraction (XRD, Rigaku Ultima IV) with Cu Kα radiation. Particle morphology was observed by scanning electron microscopy (SEM, Hitachi S-3500N) and transmission electron microscopy (TEM, JEOL 2100). Energy diffraction patterns were obtained through selected area electron diffraction (SAED). The residual carbon content was determined by an elemental analyzer (Vario Micro Cube).

Electrochemical properties of the $Li_3V_2(PO_4)_3$/C composite was evaluated using coin-type cells with a lithium foil at the negative electrode and $Li_3V_2(PO_4)_3$/C composites at the positive electrode. To make composite electrodes, the as-prepared powders (75 wt.%) with acetylene black (15 wt.%) and polyvinylidiene fluoride (PVDF) binder (10 wt.%) were mixed homogeneously. The obtained slurry was then coated uniformly on an aluminum foil, and dried at 80 °C overnight in vacuum. The electrolyte was 1 M $LiPF_6$ solution in EC/DMC/EMC (1:1:1 in weight) while Celgard 2300 was used as electrode separator. The cells were assembled in an argon-filled glove box. Galvanostatic cycling was performed between cut-off voltages of 3.0 and 4.3 V (vs. Li/Li^+) on a Land CT2001A battery tester. Cyclic voltammetry (CV) and potentiostatic intermittent titration (PITT) measurements were carried out on a CHI660c Electrochemical Workstation. The CV data was recorded between 3.0 and 4.3 V (vs. Li/Li^+) at various scan rates. For PITT tests, 10–20 mV potential steps were applied during the charge process. All electrochemical tests were conducted at room temperature.

3. Results and discussion

The X-ray diffractogram of the product is shown in Fig. 1. The pattern is consistent with reliable literature sources [1,26]. The diffraction peaks can be indexed to a monoclinic structure (space group $P2_1/n$). The lattice parameters are calculated to be $a = 8.6225$ Å, $b = 8.5506$ Å, $c = 11.9800$ Å, and $\beta = 90.44°$, which compare favorably with those in previous reports [1,26]. Element analysis (EA) of the product reveals a carbon content of 6.7 wt.%. However, carbon is not reflected in diffraction peaks. Carbon was generated from pyrolyzed organic precursor during heat treatment and might exist in amorphous form.

Fig. 2 shows the SEM image of $Li_3V_2(PO_4)_3$/C particles. It can be observed that the particles vary in size and some submicron-sized particles aggregate to form secondary particles. The TEM image (Fig. 3a) shows the particle size is ca. 200–300 nm. In addition, the particles appear to be packed by smaller nanosheets, judging from the brightness. The light-gray sponge-like webs linked to the particle edge are formed by residual carbons. By observing the edge of one particle we could also find the presence of carbon layer, as seen in Fig. 3b. The amorphous nature of carbon and the crystal nature of $Li_3V_2(PO_4)_3$ are both evidenced by the SAED patterns (Fig. 3d and c). It demonstrates that the carbon also deposits on the particle surface. According to the Salah et al. [27], pyrolysis of organic compounds under high temperature will generate predominantly graphitic carbon, which is the only carbon type that can be conductive. The bulk conductivity increases accordingly, and the polarization of the composite electrode could be minimized. Moreover, the mesostructure of pyrolyzed carbon is favorable for Li^+ transport.

Electrochemical charge/discharge profiles and rate performance for $Li_3V_2(PO_4)_3$/C cycled at various current densities (ca. 1–30 C) are shown in Fig. 4. Herein a rate of *nC* denotes to a full charge or discharge in $1/n$ h. Typical voltage profiles of $Li_3V_2(PO_4)_3$ containing three pairs of flat plateaus could be seen from 1 to 5 C (see Fig. 4a). The voltage profiles obtained between 3.0 and 4.3 V correspond to the V^{3+}/V^{4+} redox couple.

During the charge process, the voltage profiles display three flat plateaus located around 3.59, 3.68, and 4.08 V, corresponding to the first-order transitions of $Li_{3-x}V_2(PO_4)_3$. The first two plateaus are in accordance with the extraction of first Li ($Li_3V_2(PO_4)_3 \rightarrow Li_2V_2(PO_4)_3$), while the third long plateau is related to the extraction of second Li ($Li_2V_2(PO_4)_3 \rightarrow LiV_2(PO_4)_3$). During the discharge process, three flat plateaus can be seen at 4.04, 3.65 and 3.57 V, corresponding to the reversed two-phase transitions. $LiV_2(PO_4)_3$ is re-inserted with two Li in this process. It can be seen from these curves that the cell voltage difference magnifies and the capacities decrease with increasing charge/discharge rates. Meanwhile, the two plateaus around 3.6 V merge into one and flat plateaus gradually disappear.

It was reported that monoclinic $Li_3V_2(PO_4)_3$ owns a 3-D structure, allowing rapid ion transport similar to the NASICON phases [1,28]. This nature is proved by rate performance tests, as shown in Fig. 4b. The capacity retention keeps good for all current densities applied to the cell. The discharge capacity at 1 C is 124 mAh g^{-1}. As the rate is raised to 2, 5 and 10 C, the cell delivers a capacity of 123, 122 and 120 mAh g^{-1}, respectively. Note that the capacity loss is less than 4% from 1 to 10 C. At a high rate of 20 C (2178 mA g^{-1}), a capacity of 115 mAh g^{-1} is obtained. Even at the highest 30 C (3373 mA g^{-1}) rate, that is 2 min discharge, the capacity is above 100 mAh g^{-1}, which is about 82% of its initial value at 1 C. Furthermore, the cell almost fully retrieves its lost capacity when the rate is returned to 1 C. Based on the rate capability of the composite

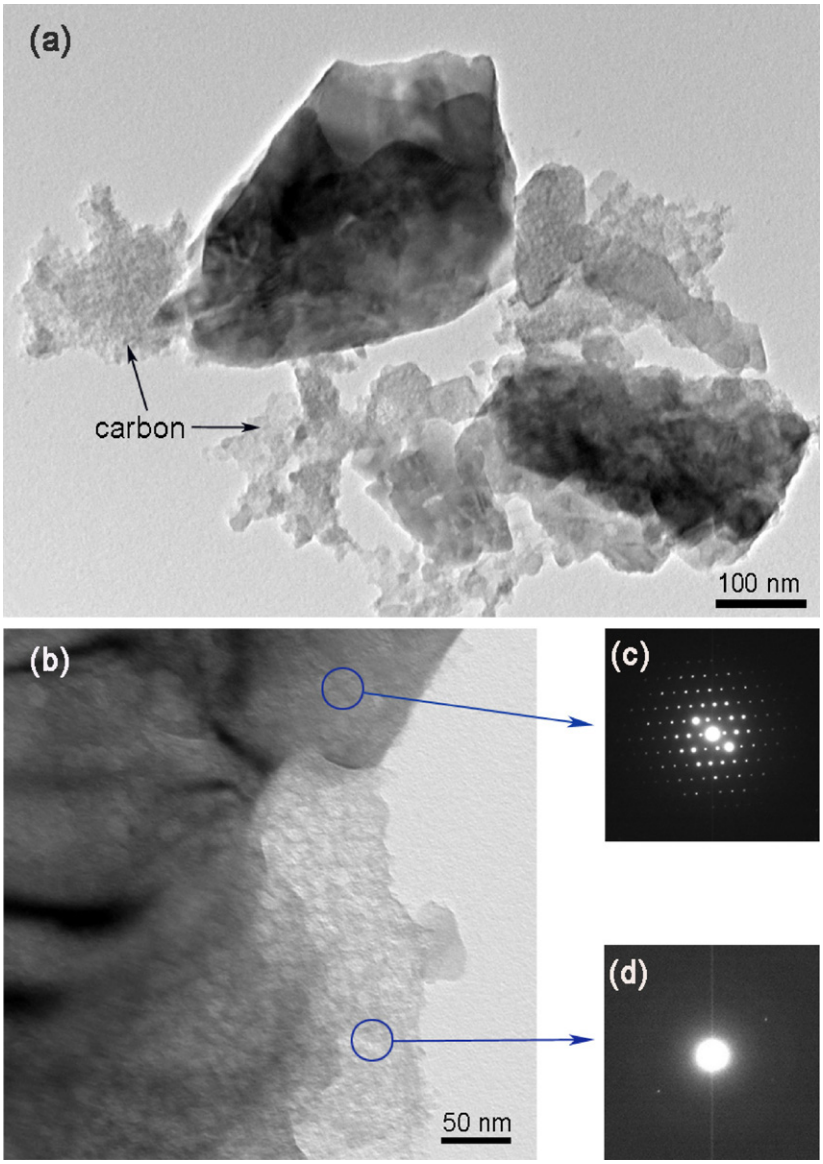

Fig. 3. (a) TEM image of $Li_3V_2(PO_4)_3$/C particles; (b)–(d) TEM image showing the edge of one particle and the corresponding SAED patterns.

electrode, $Li_3V_2(PO_4)_3$ is a promising cathode material for high-rate lithium-ion batteries.

Our results indicate that there is no need to dope $Li_3V_2(PO_4)_3$ with alien cations for acquiring satisfying rate capability, thus simplifying preparation procedures. By adding organic precursor into the raw materials and using the rheological phase method, high-rate $Li_3V_2(PO_4)_3$ could be prepared with intimate mixing wit carbon. This finding may be meaningful for large-scale applications such as electrical vehicles (EVs) and hybrid electrical vehicles (HEVs).

To understand the kinetic properties of the material under electrochemical tests, we adopted CV and PITT methods to analyze the Li^+ transport. CV technique is a typical method for the evaluation of chemical diffusion coefficients in electrode materials [29]. Fig. 5 presents a series of cyclic voltammograms of the $Li_3V_2(PO_4)_3$/C electrode at different scan rates (0.05–0.8 mV s^{-1}) in the voltage range of 3.0–4.3 V. The good symmetry of three pairs of redox peaks signifies nice reversibility. The three anodic peaks correspond to the three-step extraction of Li^+ from $Li_xV_2(PO_4)_3$, whereas the cathodic peaks are related to the re-insertion of Li^+. As the scan rate increases, the peak current also increases, with anodic peaks shifting to higher potentials and cathodic peaks shifting to lower potentials. In the case of semi-infinite and finite diffusion, the peak current I_p is proportional to the square root of scan rate $v^{1/2}$. Therefore, the chemical diffusion coefficient of Li^+ can be calculated from the Randles–Sevcik equation [30]:

$$I_p = 2.69 \times 10^5 n^{3/2} A D_{Li}{}^{1/2} v^{1/2} \Delta C \quad (1)$$

where n is the number of electrons per reaction species (for Li^+ it is 1), A is the surface area of the electrode, D_{Li} is the diffusion coefficient of Li^+, v is the scan rate, and ΔC is the change in Li^+ concentration corresponding to the specific reaction. It is assumed that the intercalation process is controlled by the solid-state diffusion of Li ions [31]. At low scan rates, I_p increases linearly with $v^{1/2}$, as shown in Fig. 6. From the slope of the linear fit, the apparent Li^+ diffusion coefficients for peak A1, A3, C2, and C3 (marked in Fig. 5) are calculated to be 2.60×10^{-9}, 1.36×10^{-9}, 2.30×10^{-9}, and 1.02×10^{-9} cm^2 s^{-1}, respectively. Peak A2 and C1 were not chosen to calculate D_{Li} for simplicity because they overlay their preceding peaks. The order of D_{Li} here is much higher than that of $LiFePO_4$ [22]. Li^+ diffusion coefficient is a key factor reflecting the Li^+ intercalation

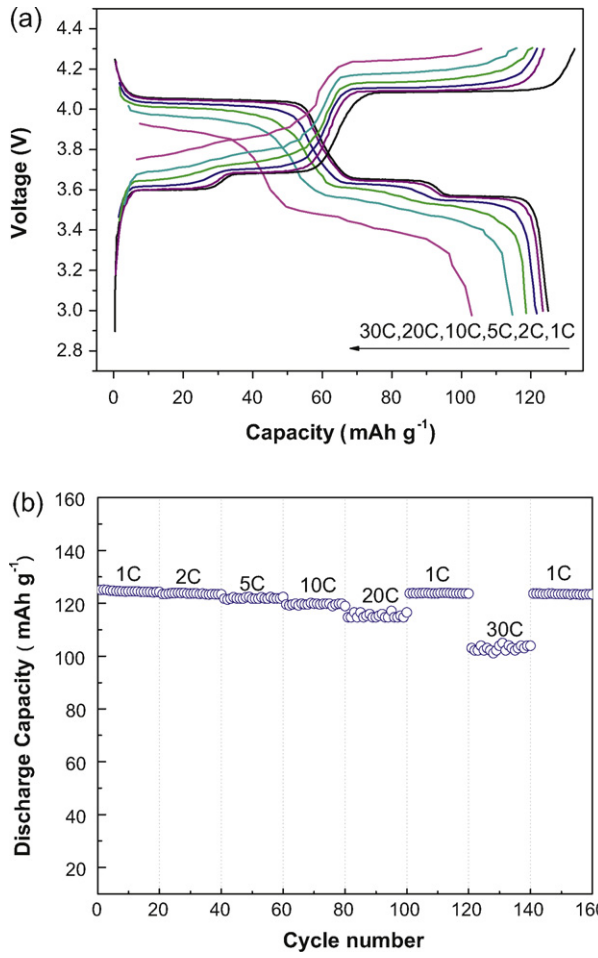

Fig. 4. (a) Charge/discharge profiles and (b) rate performance of $Li_3V_2(PO_4)_3$/C at various C-rates.

behavior in the electrode. Higher diffusion coefficient means faster insertion/extraction of Li^+ ions and hence better rate performance.

PITT method was applied to obtained highly resolved data on Li^+ diffusion coefficients. Detailed discussions of PITT can be found in previous literature [32,33]. In brief, a chronoamperometric response can be obtained after a potential step. After plotting $It^{1/2}$ vs. log t which reflects several kinetic regions, the diffusion

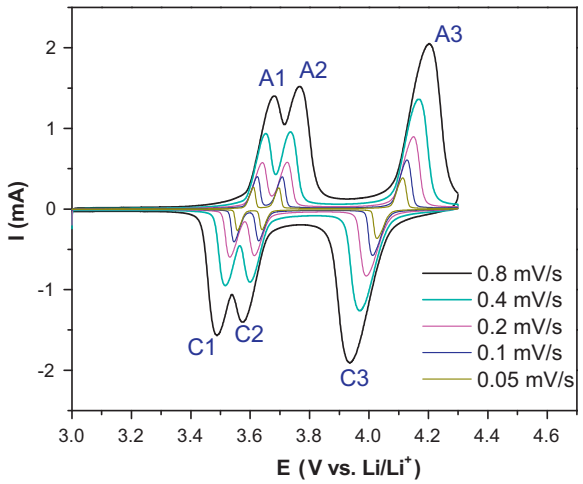

Fig. 5. Cyclic voltammograms of the $Li_3V_2(PO_4)_3$/C electrode at various scan rates.

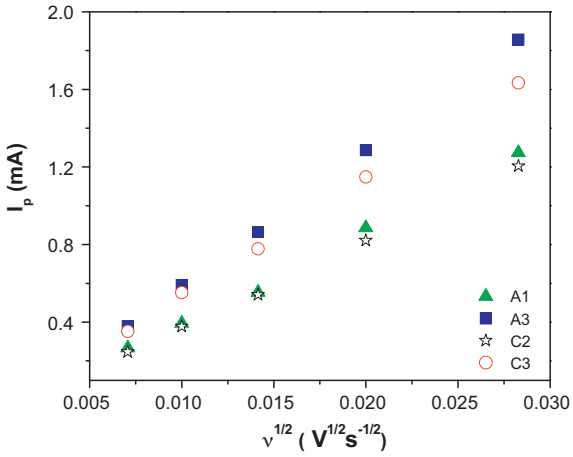

Fig. 6. The relationship of I_p to $v^{1/2}$ from the data of CV.

coefficient can be calculated from the minimum in the plot using the following equation [33]:

$$It^{1/2} = \frac{D_{Li}{}^{1/2}\Delta Q}{L\pi^{1/2}} \quad (2)$$

where D_{Li} is the diffusion coefficient of Li^+ in the bulk material, ΔQ is the total charge injected into the electrode during the potential step, and L is the characteristic diffusion length, which is assumed to be equal to the electrode thickness for simplicity.

In the long time approximation ($t > L^2/D_{Li}$), D_{Li} can be evaluated according to the following equation [26]:

$$I = \frac{2\Delta Q D_{Li}}{L^2} \exp\left(-\frac{\pi^2 D_{Li} t}{4L^2}\right) \quad (3)$$

which can be transformed to:

$$\ln\ I = \ln\left(\frac{2\Delta Q D_{Li}}{L^2}\right) - \left(\frac{\pi^2 D_{Li}}{4L^2}\right) t \quad (4)$$

Eq. (4) clearly shows that D_{Li} can be calculated from the intercept or the slope of ln I vs. t. The latter does not need to know ΔQ and is simpler in calculation.

Fig. 7a shows the current–time relationship after a 20 mV potential step from 3.485 to 3.505 V (vs. Li/Li^+). The corresponding plot of $It^{1/2}$ vs. log t is shown in Fig. 7b. The plateau in Fig. 7b reflects the Cottrell behavior. In the Cottrell region, the semi-infinite planar diffusion of lithium ions in the $Li_3V_2(PO_4)_3$ structure plays a major role. The diffusion coefficient calculated from the minimum is 4.69×10^{-7} cm^2 s^{-1}. The corresponding plot of ln I vs. t is shown in Fig. 7c. After the linear fitting, the diffusion coefficient of Li^+ is calculated to be 5.60×10^{-7} cm^2 s^{-1} from the intercept, and 3.48×10^{-7} cm^2 s^{-1} from the slope. The three values match quite well.

In the vicinity of the plateau regions (see Fig. 4a), the potential step is reduced to 10 mV. Fig. 8a shows the current–time relationship after a potential step from 4.063 to 4.073 V. It can been seen that the electrode needs more time to return to equilibrium. To calculate D_{Li}, plot of $It^{1/2}$ vs. log t is shown in Fig. 8b and plot of ln I vs. t is shown in Fig. 8c.

The chemical diffusion coefficients of Li^+ ions obtained by PITT are shown in Fig. 9a. D_{Li} ranges from 10^{-7} to 10^{-8} cm^2 s^{-1}, depending on the potentials. The values are close to the data in previous reports [3,34]. The plot displays three valleys and the minimum values coincide with the peaks in the incremental capacity curve (Fig. 9b). In addition, the three minima also correspond to the plateaus in voltage profiles (Fig. 4a). The value of D_{Li} decreases drastically as the potential moves close to the plateau regions and

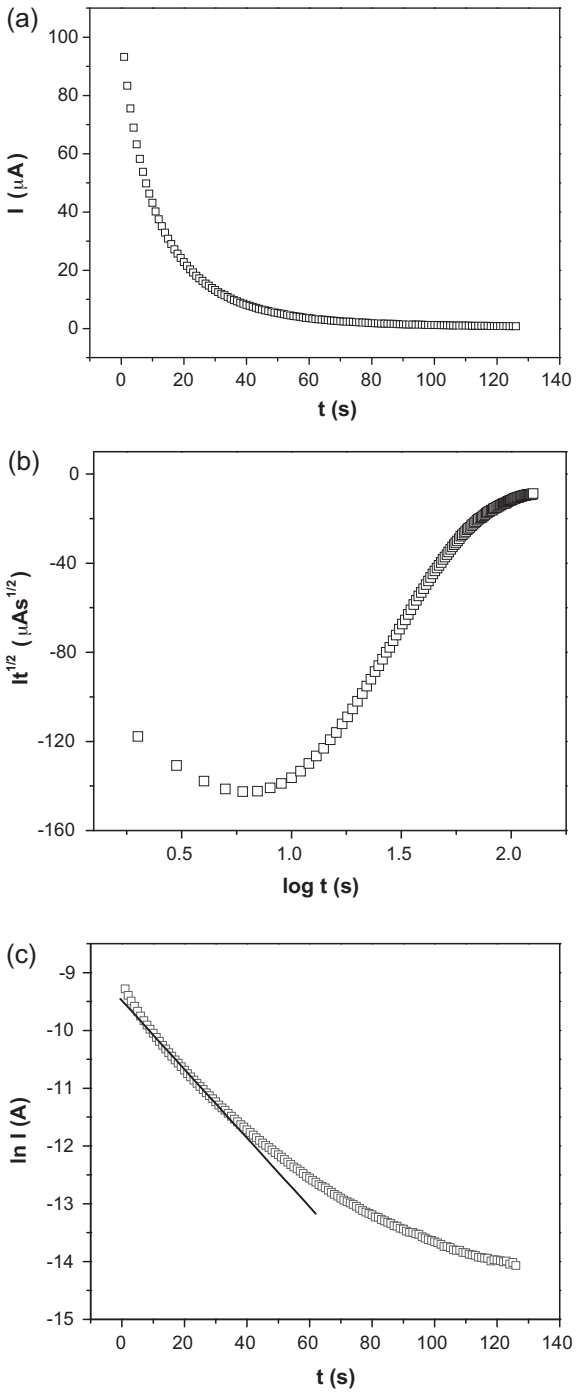

Fig. 7. (a) Current–time relationship after a 20 mV potential step from 3.485 to 3.505 V; (b) plot of $It^{1/2}$ vs. log t and (c) plot of ln I vs. t after the potential step from 3.485 to 3.505 V.

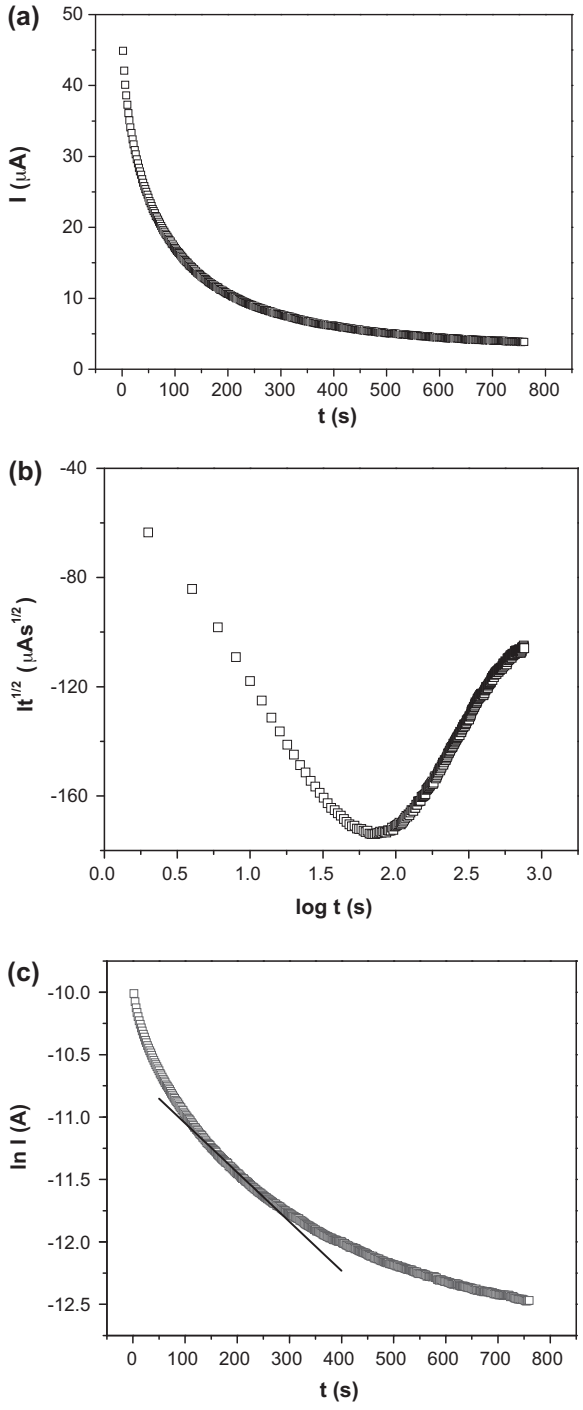

Fig. 8. (a) Current–time relationship after a 10 mV potential step from 4.063 to 4.073 V; (b) plot of $It^{1/2}$ vs. log t and (c) plot of ln I vs. t after the potential step from 4.063 to 4.073 V.

increases immediately after passing these regions. A possible explanation is that the plateau regions are actually two-phase regions for $Li_xV_2(PO_4)_3$, and Li^+ transfer in these regions is more difficult than in single phase structure [34]. For example, the first plateau during charge begins at 3.58 V and ends at 3.61 V. $Li_3V_2(PO_4)_3$ and $Li_{2.5}V_2(PO_4)_3$ coexist in this region. Before this region, D_{Li} drops from 3.15×10^{-7} cm^2 s^{-1} at 3.542 V to 3.18×10^{-8} cm^2 s^{-1} at 3.573 V, as the $Li_{2.5}V_2(PO_4)_3$ phase begins to form. After the complete transformation of $Li_3V_2(PO_4)_3$ into $Li_{2.5}V_2(PO_4)_3$, D_{Li} increases markedly to 3.15×10^{-7} cm^2 s^{-1} at 3.616 V.

The Li^+ transport is quickly slowed down in two-phase domains because of strong attractive interactions between the intercalated species [22]. In the $Li_xV_2(PO_4)_3$ system, however, the attractive interactions seem weaker than that in the Li_xFePO_4 system. On the other hand, similar to $LiFePO_4$, phosphate hosts such as $LiVOPO_4$ and $LiVPO_4F$, are also quite sensitive to rate variation [35,36]. This could be attributed to the reduced ionic/electronic conductivity of the fully extracted phase. Therefore, we think the partial use of lithium ions from $Li_3V_2(PO_4)_3$ is contributive to the good reversibility in our case.

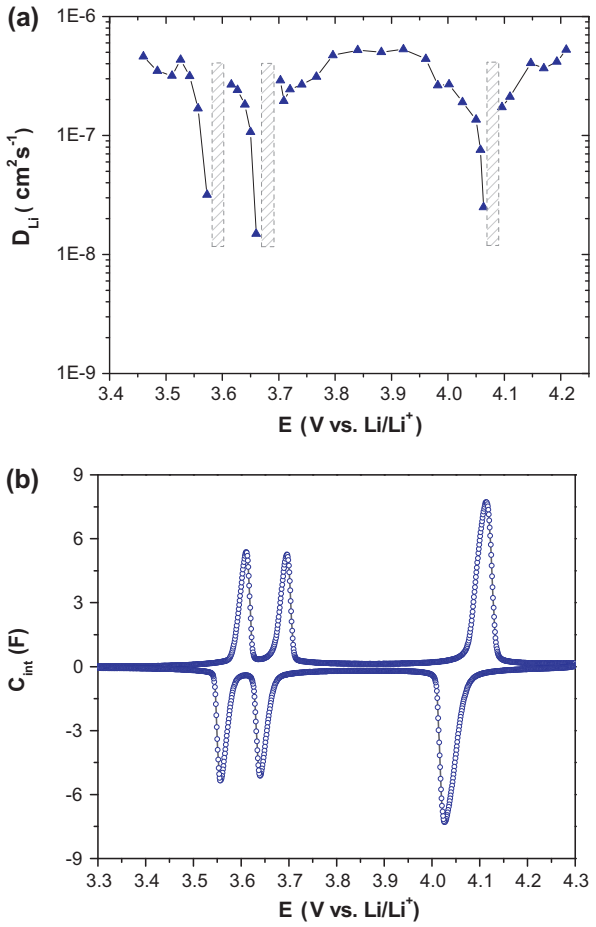

Fig. 9. (a) Dependence of Li^+ diffusion coefficient on potential, obtained by PITT; (b) Plot of incremental capacity vs. potential, obtained from CV at 0.05 mV s^{-1}.

As for the large-scale applications of battery systems, reproductibility and simplified preparation procedures are crucial to reduce costs. We noticed that some materials need complicated particle modifications or strict size control to ensure acceptable rate capability. Encouragingly, our results provide a preferable choice. The NASICON-like $Li_3V_2(PO_4)_3$ prepared by rheological phase method displayed its competence as a cathode material for high-power lithium-ion batteries, which could be used in EV/HEV batteries. The facile preparation method is feasible for scale-up production. In addition, the values of evaluated by CV and PITT measurements confirmed the good Li^+ ion mobility of $Li_3V_2(PO_4)_3$.

4. Conclusions

In summary, monoclinic $Li_3V_2(PO_4)_3$/C prepared by rheological phase method exhibited good reversibility and excellent rate capability in the voltage range of 3.0–4.3 V, corresponding to the utilization the V^{3+}/V^{4+} redox couple. The results showed that the composite achieved its theoretical capacity at the 1 C rate. The capacity fade was less than 4% from 1 to 10 C. In addition, a capacity of above 100 mAh g^{-1} was obtained at the 30 C rate, with negligible deterioration of the cell. The reversibility of the material was confirmed by the good symmetry of the redox peaks in CV curves. The Li^+ diffusion coefficients calculated from PITT ranged from 10^{-7} to 10^{-8} cm^2 s^{-1}, depending on the potentials. The efficient rheological phase method, together with the intrinsic fast Li^+ mobility and the partial use of Li from $Li_3V_2(PO_4)_3$, are considered to be the reason for satisfactory reversibility of $Li_3V_2(PO_4)_3$/C composite under varying current densities.

Acknowledgments

This work was supported by National 973 Program of China (No. 2009CB220100), National 863 Program of China (No. 2008AA11A104), Beijing Nova Program (No. 2009A23) and open fund of Beijing Key Laboratory of Environment Science and Engineering.

References

[1] H. Huang, S.C. Yin, T. Kerr, N. Taylor, L.F. Nazar, Adv. Mater. 14 (2002) 1525.
[2] S. Patoux, C. Wurm, M. Morcrette, G. Rousse, C. Masquelier, J. Power Sources 119–121 (2003) 278.
[3] A. Tang, X. Wang, G. Xu, R. Peng, H. Nie, Mater. Lett. 63 (2009) 2396.
[4] L. Wang, L.-C. Zhang, I. Lieberwirth, H.-W. Xu, C.-H. Chen, Electrochem. Commun. 12 (2010) 52.
[5] Y.Q. Qiao, J.P. Tu, Y.J. Mai, L.J. Cheng, X.L. Wang, C.D. Gu, J. Alloys Compd. 509 (2011) 7181.
[6] A.K. Padhi, K.S. Nanjundaswamy, J.B. Goodenough, J. Electrochem. Soc. 144 (1997) 1188.
[7] M.M. Ren, Z. Zhou, X.P. Gao, W.X. Peng, J.P. Wei, J. Phys. Chem. C 112 (2008) 5689.
[8] X.Y. Wang, S.Y. Yin, K.L. Zhang, Y.X. Zhang, J. Alloys Compd. 486 (2009) L5.
[9] J. Wang, X. Zhang, J. Liu, G. Yang, Y. Ge, Z. Yu, R. Wang, X. Pan, Electrochim. Acta 55 (2010) 6879.
[10] L. Wang, X. Jiang, X. Li, X. Pi, Y. Ren, F. Wu, Electrochim. Acta 55 (2010) 5057.
[11] Y.N. Ko, H.Y. Koo, J.H. Kim, J.H. Yi, Y.C. Kang, J.-H. Lee, J. Power Sources 196 (2011) 6682.
[12] Y.Q. Qiao, J.P. Tu, J.Y. Xiang, X.L. Wang, Y.J. Mai, D. Zhang, W.L. Liu, Electrochim. Acta 56 (2011) 4139.
[13] Y.Q. Qiao, X.L. Wang, Y.J. Mai, J.Y. Xiang, D. Zhang, C.D. Gu, J.P. Tu, J. Power Sources 196 (2011) 8706.
[14] G. Yang, H. Liu, H. Ji, Z. Chen, X. Jiang, J. Power Sources 195 (2010) 5374.
[15] B. Huang, X. Fan, X. Zheng, M. Lu, J. Alloys Compd. 509 (2011) 4765.
[16] H. Liu, C. Cheng, X. Huang, J. Li, Electrochim. Acta 55 (2010) 8461.
[17] S.C. Yin, H. Grondey, P. Strobel, M. Anne, L.F. Nazar, J. Am. Chem. Soc. 125 (2003) 10402.
[18] M. Morcrette, J.B. Leriche, S. Patoux, C. Wurm, C. Masquelier, Electrochem. Solid-State Lett. 6 (2003) A80.
[19] M.D. Levi, K. Gamolsky, D. Aurbach, U. Heider, R. Oesten, J. Electroanal. Chem. 477 (1999) 32.
[20] Y.H. Rho, K. Kanamura, J. Solid State Chem. 177 (2004) 2094.
[21] A.V. Churikov, A.V. Ivanishchev, I.A. Ivanishcheva, V.O. Sycheva, N.R. Khasanova, E.V. Antipov, Electrochim. Acta 55 (2010) 2939.
[22] P.P. Prosini, M. Lisi, D. Zane, M. Pasquali, Solid State Ionics 148 (2002) 45.
[23] J. Sun, W. Xie, L. Yuan, K. Zhang, Q. Wang, Mater. Sci. Eng B64 (1999) 157.
[24] C. Wang, X. Ma, Z. Li, Y. Liang, J. Sun, Y. Zhou, Electrochem. Commun. 8 (2006) 289.
[25] C. Chang, J. Xiang, X. Shi, X. Han, L. Yuan, J. Sun, Electrochim. Acta 53 (2008) 2232.
[26] J. Barker, M.Y. Saidi, J.L. Swoyer, J. Electrochem. Soc. 150 (2003) A684.
[27] A.A. Salah, A. Mauger, K. Zaghib, J.B. Goodenough, N. Ravet, M. Gauthier, F. Gendron, C.M. Julien, J. Electrochem. Soc. 153 (2006) A1692.
[28] M.Y. Saïdi, J. Barker, H. Huang, J.L. Swoyer, G. Adamson, J. Power Sources 119–121 (2003) 266.
[29] D.Y.W. Yu, C. Fietzek, W. Weydanz, K. Donoue, T. Inoue, H. Kurokawa, S. Fujitani, J. Electrochem. Soc. 154 (2007) A253.
[30] S.R. Das, S.B. Majumder, R.S. Katiyar, J. Power Sources 139 (2005) 261.
[31] Y. Xia, H. Takeshige, H. Noguchi, M. Yoshio, J. Power Sources 56 (1995) 61.
[32] C.J. Wen, B.A. Boukamp, R.A. Huggins, W. Weppner, J. Electrochem. Soc. 126 (1979) 2258.
[33] M.D. Levi, E.A. Levi, D. Aurbach, J. Electroanal. Chem. 421 (1997) 89.
[34] S.-Q. Liu, S.-C. Li, K.-L. Huang, B.-L. Gong, G. Zhang, J. Alloys Compd. 450 (2008) 499.
[35] B.M. Azmi, T. Ishihara, H. Nishiguchi, Y. Takita, J. Power Sources 146 (2005) 525.
[36] R.K.B. Gover, P. Burns, A. Bryan, M.Y. Saidi, J.L. Swoyer, J. Barker, Solid State Ionics 177 (2006) 2635.